Growth of polycrystalline Pr4Ni3O10 thin films for intermediate temperature solid oxide fuel cell cathode by radio frequency magnetron co-sputtering

Patrick Laffez, Quentin Simon, Yuhei Kikuchi, Richard Retoux, Fabien Giovannelli, Ayako Yamamoto

Growth of polycrystalline $Pr_4Ni_3O_{10}$ thin films for intermediate temperature solid oxide fuel cell cathode by radio frequency magnetron co-sputtering

Patrick, LAFFEZ[a], Quentin SIMON[a], Yuhei KIKUCHI[a,b], Richard RETOUX[c], Fabien GIOVANNELLI[a], Ayako YAMAMOTO[b].*

a) *University of Tours, GREMAN, UMR 7347– CNRS, IUT de Blois 15 rue de la chocolaterie CS 2903, 41029 Blois Cedex, FRANCE*
b) *Shibaura Institute of Technology, Graduate School of Science & Technology, Toyosu 3-7-5, Koto-ku, 135-8548, Tokyo, Japan*
c) *CRISMAT, Laboratoire de Cristallographie et Sciences des Matériaux, UMR6508, Normandie Univ, ENSICAEN, UNICAEN, CNRS, 6 Bd Maréchal Juin, F-14050 Caen 4 France*

**corresponding author, patrick.laffez@univ-tours.fr*

Key words: Solid Oxide Fuel Cell; praseodymium nickelate; sputtering

Abstract

The performances of Solid Oxide Fuel Cells (SOFC) are strongly related to the catalytic/conductive properties of cathode materials, which are temperature dependent. The optimal temperature in operating conditions implies a tradeoff between high efficiency at high temperatures and improved lifetime at Intermediate Temperatures (IT). Among the candidates, Pr_2NiO_4 presents attractive functional properties but is susceptible to decompose into $Pr_4Ni_3O_{10}$ under IT-SOFC conditions. In this contribution, a deposition process to obtain $Pr_4Ni_3O_{10}$ phase were directly targeted as a potential alternative to the integration of Pr_2NiO_4 in IT-SOFC. $Pr_4Ni_3O_{10}$ thin films have been deposited on Y-stabilized Zirconia substrates through a two-step process: i) room temperature co-sputtering of metallic Ni and Pr targets, ii) ex-situ annealing under O_2 flux. The composition of thin films were adjusted by changing the power applied to each target and confirmed by Energy Dispersive Spectroscopy. X-Ray Diffraction analyses as a function of temperature were made to identify the temperature window to stabilize the desired phase. The structural and morphological features of polycrystalline $Pr_4Ni_3O_{10}$ thin films were analyzed by Transmission Electron Microscopy and Scanning Electron Microscopy. Electrical resistivity of ~$6.5.10^{-3}$ Ω.cm and Seebeck coefficient of ~ – 23 μV.K^{-1} at 150°C highlight the synthesis of $Pr_4Ni_3O_{10}$ continuous coatings representing a promising candidate for cathodes in IT-SOFC.

1. Introduction

Rare-earth Nickelates have peculiar exotic magnetic, electrical and infrared optical properties. Perovskite $RNiO_3$ (R : rare earth) are well known for their metal-insulator transition versus temperature [1-2]. R_2NiO_4, derivates from the perovskite structure belonging to the Ruddlesden-Popper series with n=1 in the general formula $R_{n+1}Ni_nO_{3n+1}$, show interesting properties such as high emissivity in the infrared range [3] as well as Mixed Ionic and Electronic Conductivity (MIEC) [4-5]. The ionic conductivity, *i.e.* the high capacity to absorb and to diffuse interstitial oxygen within their structure, makes these compounds some of the best candidates for cathode materials in Solid Oxide Fuel Cells (SOFC) [6].

The performances of SOFC are strongly related to the catalytic/conductive properties of cathode materials, which are temperature dependent. For practical application, the optimal operating conditions imply a tradeoff between high efficiency at high temperatures and improved lifespan at low temperatures. The current trend is to reduce the operating conditions from 800°C-1000°C to intermediate temperature (IT) range, typically 500°C-800°C.

Among the $R_2NiO_{4\pm\delta}$ candidates (R = La, Pr, Nd), compounds with R = Pr, where valence of Ni can fluctuate between II and III [7], have been identified as the most promising materials for SOFC applications [8]. In a recent work, Fondard *et al.* studied the synthesis parameters of R_2NiO_4 (R = La, Pr, Nd) thin films by reactive magnetron sputtering [9]. The authors confirmed the high ionic and electron conductivity of these phases, and their potential interest for SOFC cathode, especially the praseodymium nickelate coatings. However, due to its instability at intermediate temperature, Pr_2NiO_4 needs synthesis temperature as high as 1100°C, which makes it unstable at the operating SOFC temperature. It is therefore challenging to investigate alternative materials that could combine good functional properties together with long-term stability.

In the Ruddlesden-Popper series $R_{n+1}Ni_nO_{3n+1}$, recent attention was brought to compounds with n = 3 ($R_4Ni_3O_{10}$) because of their superior stability compared to R_2NiO_4 compounds from moderate to high temperatures, along with attractive electro-chemical performances. For example, for lanthanum compounds, Amov et *al.* suggest that La_2NiO_4 is less stable than compounds with n = 2 or 3 for long time exposure at 900°C [10]. Sharma et *al.* synthesized at 950°C the $La_4Ni_3O_{10}$ phase endowed by polarization resistance values of R_p = 2.01 $\Omega.cm^2$ at 600°C [11]. Regarding praseodymium compounds, Kovalesky *et al.* have reported that Pr_2NiO_4 decomposes into $Pr_4Ni_3O_{10}$ and PrO_x in the 800-950°C range [12] and Vibhu *et al.* reported that Pr_2NiO_4 decomposes into $PrNiO_3$, $Pr_4Ni_3O_{10}$ and Pr_6O_{11} in the 600-800°C range [13]. Vibhu et *al.* also recently showed on bulk $Pr_4Ni_3O_{10}$ ceramics, promising properties as oxygen electrode with, for example, polarization resistance of R_p = 0.16 $\Omega.cm^2$ at 600°C. These performances are comparable to Pr_2NiO_4 [14]. It is suggested that $Pr_4Ni_3O_{10}$ is a MIEC under oxygen and air up to 1000 °C. The authors have also showed that in the 600°C-800°C range, $Pr_4Ni_3O_{10}$ was stable in air for at least one month. In addition, $Pr_4Ni_3O_{10}$ phase was found to be stable up to 1050°C in air and up to 1120°C in oxygen.

Therefore, $Pr_4Ni_3O_{10}$ is an excellent candidate for advanced industrial applications. Yet a reproducible and standardized synthesis method is required for coating deposition. Among physical vapor deposition techniques, magnetron sputtering is a versatile one, suitable for high quality coatings with good adhesion of a wide range of materials at commercially useful rates and environmentally-friendly. The current work presents the optimization conditions of $Pr_4Ni_3O_{10}$ coatings by Radio Frequency (RF) magnetron sputtering and post-annealing treatment with particular attention to the phase formation and the microstructure of coatings.

2. Experimental part : Synthesis and characterizations

The experimental procedure was adapted from previous work [3]. The sputtering experimental chamber combines a primary pump with a turbo molecular pump enabling base pressure to drop to 10^{-5} Pa. The co-sputtering chamber is equipped with a rotating and heating substrate holder. Two 50 millimeter magnetron cathodes in a converging configuration are equipped with a praseodymium (99.9%) and a nickel (99.5%) target.

The electrical RF power applied to the Pr and Ni targets can be independently controlled and can vary between 10 W and 150 W in order to accurately adjust the Pr/Ni ratio to 4/3 (57% Pr, 43% Ni), corresponding to the $Pr_4Ni_3O_{10}$ formula. The argon flux is fixed at 25 sccm during plasma sputtering. The working pressure was controlled from 0.5 to 5.0 Pa by adjusting the aperture between the chamber and the turbo molecular pump. Films were deposited for 45 minutes with the substrate holder at room temperature, 400°C or 600°C. Films were grown on ceramic alumina (Al_2O_3) and Yttrium stabilized zirconia (YSZ) $Zr_{0.95}Y_{0.05}O_{2-x}$ mirror polished substrates. These substrates were polycrystalline and did not present any preferential orientation. Post annealing were carried out up to 1100° C in a tubular furnace under oxygen flux at a pressure of 10^5 Pa).

The chemical composition was checked by Energy Dispersive X-ray spectroscopy at 15 kV (EDX, Oxford Instrument AZTec). Surface topography was determined using scanning electron microscopy (SEM, TESCAN) working with a Field Emission Gun (FEG) operating at 10 kV. X-ray diffraction (XRD) was performed using a Bruker diffractometer D8 advance twin-twin, using Kα(Cu) radiation (λ = 1.5418 Å). XRD patterns at various temperatures were recorded in Bragg Brentano θ - 2θ configuration using a heating device from 50 °C to 1200 °C with a 50°C increment, and a plateau of 1h for each temperature. Phase identification and unit cell refinement were done using the EVA software (Bruker corp.) and CELREF X-ray diffraction software respectively [15]. Grazing Incidence XRD (GI-XRD) were also made on the same diffractometer using an X-ray parallel beam with a fixed incident angle of 1°.

Transmission Electron Microscopy was carried out at room temperature. Specimens for TEM observations were prepared by scraping the thin films in ethanol using a diamond knife. A drop of the suspension was deposited and dried onto a carbon coated copper grid. High Resolution Transmission Electron Microscopy (HRTEM) and Electron Diffraction (ED) study of the scraped samples were done on a 200 kV JEOL 2010 FEG electron microscope (tilt ± 42°).

Electrical conductivity and the Seebeck coefficient were measured simultaneously by ULVAC ZEM3 in a low pressure He atmosphere from 80°C to 220°C.

3. Results and Discussion

3.1 Optimization of the film composition

It is challenging with convergent targets to determine the best proper RF power to use on each target in order to obtain the desired stoichiometry. Other intrinsic and extrinsic parameters such as argon pressure, substrate temperature or target-substrate distance can also affect the composition, the microstructure, and the crystal structure of the film. Consequently, an optimization of the growth conditions is essential to obtain the desired atomic composition, 57% Pr, 43% Ni.

The auto-polarization voltage of the targets measured during the RF sputtering processes (called hereafter bias voltage) is very sensitive to the above-mentioned parameters. The bias voltage is considered to be a valuable feedback to monitor for process optimization and especially regarding the pre-sputtering stage of metal targets sensitive to oxidation.

In a previous work [3], we adjusted the deposition condition for Pr_2NiO_4 material at 1.5 Pa argon using a single composite target and optimizing the surface ratio of the two metals. It was observed that the chemical composition variation *versus* RF power density was not linear. Above 0.953 W/cm^2, the praseodymium deposition rate becomes high, along with a color change of the plasma from pink to green, related to the high concentration of Pr^{3+}. Similar behavior can be observed after a certain time of sputtering while keeping a constant and lower power density on the Pr target: a plasma color change, accompanied by an increase in the bias voltage. After a while, the Pr plasma is definitely green and the bias voltage is stabilized. It this establishes that the color change associated with a modification of the surface electrical conductivity of the target is likely due to the removal of a poisoning superficial oxide layer upon this pre-sputtering step. In the present work, we always formatted the Pr target for a sufficient time to ensure a fully metallic surface. Regarding the strong dependence of the sputtering yield with voltage bias, the film composition was adjusted by varying the RF power on the two targets during the film growth. Table 1 reports typical synthesis conditions leading to the closest expected atomic ratio of 57% Pr and 43% Ni for samples deposited at a working pressure of 1.5 Pa. Note that the substrate temperature during deposition did not have influence on the thin film composition. Changing the working pressure is well known to influence both the sputtering yield of each chemical element and also to modify the microstructure of the coating [16]. This property is mainly related to the enhancement of scattering of the sputtered elements. In the present work, EDX analysis showed that an increase in working pressure leads to a monotonous evolution of the composition: increase the Pr content, decrease the Ni content. Samples deposited at 0.5 Pa and at 5 Pa presented the compositions 42% Pr, 58% Ni and 66% Pr, 34% Ni, respectively. This was confirmed by X ray diffraction, where we observed that samples deposited at 0.5 Pa showed an excess of NiO while samples at 5 Pa showed an excess of Pr_6O_{11} as discussed below.

3.2 Determination of the annealing temperature

In order to determine the annealing temperature, *in situ* temperature X-ray diffraction measurements (from 50 °C to 1200 °C with a 50°C increment) were carried out in oxygen flow on a film initially deposited on YSZ at room temperature. The results are shown in Fig. 1. At room temperature, the sample was nearly amorphous as indicated by the broad peak at 2θ = 27°. The XRD diagram made on bare substrate enables the YSZ contribution to be identified.

At 800°C, the praseodymium oxide phase appeared, characterized by the peaks at 27.86° and 32.28° (PDF card n°01-071-0341) [17]. At the same temperature NiO (PDF card n°00-004-0835) [18] was also observed, confirmed by the peaks at 37.3° and 44.29°. At 1000°C, NiO and Praseodymium oxide started to react together and their corresponding diffraction intensities decreased. At this temperature, the crystallization of the $Pr_4Ni_3O_{10}$ phase started as indicated by the appearance of reflection peaks particularly at 32.3°, 32.7°, and 33.05° (2θ) (PDF card n°00-050-0468) [19]. This phase can be indexed in an orthorhombic unit cell, using the $La_4Ni_3O_{10}$ isotype structure (PDF card n°00-050-0243) [20]. At 1050°C, the sample showed mainly $Pr_4Ni_3O_{10}$ together with a small amount of PrO_x. Above 1100°C $Pr_4Ni_3O_{10}$ started to decompose to $Pr_2NiO_{4+\delta}$ in the tetragonal form (PDF card n°00-058-0850) [21] and NiO. At 1200°C, the film showed a majority of Pr_2NiO_4. In order to minimize the formation of Pr_2NiO_4 phase, the annealing temperature should be lower than 1200 °C. As a result, the stability of $Pr_4Ni_3O_{10}$ films was found to be in the 1000°C − 1050°C range. It is also observed that the orthorhombic distortion is clearly enhanced at the higher temperature.

3.3 Structural properties

Typical GI-XRD patterns of bare YSZ substrate (a) and of samples deposited at room temperature, 1.5 Pa and annealed at 1000°C and 1025°C are shown in figures 2(b) and 2(c), respectively. In both cases, the $Pr_4Ni_3O_{10}$ phase is observed, with a small amount of unreacted Pr_6O_{11} in the first. The annealing temperature of 1025°C was chosen for the rest of this work. Similar results were obtained for samples deposited with a substrate temperature maintained at 400°C or 600°C and annealed in the same conditions (not shown here). Bragg positions of $Pr_4Ni_3O_{10}$ can be described as orthorhombic *Fmmm* (space group N° 69). The unit-cells refinement, carried out with the least square method using CELREF software, allows cell parameters to be determined and are summarized in table 2. The refined cell parameters are consistent with the previous report [14]. The GI-XRD patterns of samples deposited with working pressure of 0.5 Pa and 5 Pa are also presented in figures 2(d) and 2(e). In line with the EDX analyses, film deposited at 0.5 Pa displayed a NiO excess while film deposited at 5 Pa presented a Pr_6O_{11} excess.

Attempts to stabilize $Pr_4Ni_3O_{10}$ on alumina substrate were also done. It was observed that samples showed a reactivity between alumina and praseodymium leading to the formation of the $PrAlO_3$ perovskite, as already observed in ref [3] (not shown). For this kind of synthesis, no further investigations were undertaken.

The structural characteristics of $Pr_4Ni_3O_4$ thin films deposited at 1.5 Pa were also studied by TEM (figure 3). The cell parameters and reflection conditions deduced from Electron Diffraction of $Pr_4Ni_3O_4$ crystals scratched from the thin film are in agreement with the *Fmmm* space group used in the X ray diffraction study (figure 3a, 3b) and cell parameters are confirmed (*a* and *b* close to 5.4 Å and *c* close to 27.3Å). A typical grain size, never more than 200 nm, was observed in the $Pr_4Ni_3O_{10}$ thin films (figure 3c) while lattice images presented in figure 3d confirm of the good crystallinity of the films and the stacking of the triple NiO layer along the *c* axis [22]. Here (figure 3d) the light grey lines are representative of the NiO layers.

3.4 Morphology of annealed film

Figures 4 (a-f) display the observation by FEG-SEM of the microstructure of annealing films deposited at different pressures and different substrate temperatures. For the observation, the samples were inserted in the microscope without any metallization. The conductivity of the samples was high enough to avoid charge accumulation.

Figures 4a and 4b show the surface (Secondary electron image) and the cross section (backscattering electron image) of a sample grown on YSZ substrate at working pressure of 1.5 Pa and annealed at 1025°C. Note that the inset in figure 4a represents a plane view of bare YSZ substrate.

The plane view shows a microstructure with grain size ranging from 100 nm to 500 nm, with no roughness enabling the film microstructure to reproduce the substrate form. Residual porosity with 100 nm pores is randomly dispersed. SEM cross-section image of the layer (figure 4(b)) reveals a granular and porous growth with a thickness of 770 ± 50 nm. From this value we can estimate the deposition rate of the film. The Pilling – Bedworth ratio is defined as the ratio of the volume of the

unit cell of a metal oxide to the volume of the elementary cell of the corresponding metal from which the oxide is created [23]. It can be calculated using the relation:

$$R_{PB} = \frac{V_{oxide}}{V_{Metal}} = \frac{M_O \, \rho_M}{n \, M_M \, \rho_O}$$

where : M_O= 897.32 g, Molar Mass of oxide, M_M= 105.6 Molar Mass of metal, ρ_O= 7.31 g/cm^3 density of oxide, ρ_M= 7.68 g/cm^3 density of metal, and n = 7, number of atoms of metal per molecule of the oxide $Pr_4Ni_3O_{10}$. ρ_M and M_M are estimated by calculating the weighted average of the metallic composition, $\rho_{M=\frac{4\rho_{Pr}+3\rho_{Ni}}{7}}$ $M_{M=\frac{4M_{Pr}+3M_{Ni}}{7}}$. ρ_O and M_O are calculated using value of table 2 for the unit cell volume.

Because the surface of the sample before and after annealing is considered constant, we can estimate that the Pilling – Bedworth ratio will represent also for the film's thickness before and after annealing

$$R_{PB} = \frac{V_{oxide}}{V_{Metal}} = \frac{th_{oxide}}{th_{Metal}}$$

From these considerations, we found $R_{PB} = \frac{th_{oxide}}{th_{Metal}} = 1.27$

For a deposition time of 45 minutes, and for the annealing condition of 18 hours at 1025°C with oxygen flux, the thickness of oxide film was 770 nm, corresponding to a metal deposition of 600 nm. The corresponding metallic deposition rate is then approximated at 800 nm per hour.

Figures 4c and 4d show plan view of two samples deposited at 0.5 Pa and 5 Pa respectively. The 0.5 Pa sample was rather similar to the film made at 1.5 Pa (compared with figure 4a) with an even smoother surface. On the other hand, figure 4d shows the film deposited at 5Pa. The effect on microstructure is brought out, showing an increase in roughness in relation to the increase of the scattering of the chemical element during deposition. Finally, we have evidenced the influence of substrate temperature during the deposition process. Figure 4(e) and figure (f) report the plane view of samples deposited at 400°C and 600°C, respectively, and annealed at 1025°C. While no specific modifications were observed for the thin film deposited at 400°C compared to those deposited at room temperature, for a substrate temperature of 600°C, we observe a dense microstructure with an increase in grain size and without any apparent porosity. All these results are in agreement with Thornton phase diagram with an improvement in density as the substrate temperature increased and the Ar pressure decreased [24], as also observed on $RNiO_3$ (R = Nd) thin films deposited by DC sputtering [25]. This observation suggests that the resulting microstructure of the oxide films after annealing depends on the growth mechanism involved in the sputtering deposition of metals.

3.5 Electronic properties

The typical evolution of the electrical resistivity and the Seebeck coefficient as a function of temperature from 80°C to 220°C° are presented in figure 5 for a $Pr_4Ni_3O_{10}$ film deposited at room

temperature and 1.5 Pa followed by annealing at 1025°C in O_2 flow for 18 h. In this temperature range, the electrical resistivity slightly increased from 6.10^{-3} Ω.cm to 7.10^{-3} Ω.cm whereas the Seebeck coefficient gradually varied from – 20.4 to – 25.0 μV.K^{-1}. The negative values for the Seebeck coefficient revealed that conductivity is mainly ensured by electrons. The increase in resistivity with temperature suggested a metallic-like behavior with a reduction of charge carrier mobility with increasing temperature. One should note however that due to experimental equipment (Ni electrodes), electrical measurement was made in the atmosphere and the material may lose oxygen in the surrounding media. A slight change in charge carrier concentration therefore cannot be ruled out [14]. Compounds in the Ruddlesden-Popper series can accommodate important deviation in oxygen stoichiometry (δ value in $Pr_4Ni_3O_{10+\delta}$) which, in turn, impacts the electrical properties. Indeed, Bassat et *al.* have prepared $Pr_4Ni_3O_{10+\delta}$ bulk ceramic in various annealing conditions (from reducing to oxidizing atmosphere) leading to δ and resistivity values ranging respectively from – 1.75 to 0.1 and 3.10^3 to 8.10^{-3} Ω.cm at 300K [26]. Our results, both in terms of electrical resistivity and the Seebeck coefficient, are in agreement with the values reported for bulk ceramic $Pr_4Ni_3O_{10+\delta}$ annealed in similar conditions (1097°C in O_2 atmosphere in reference [26]) for which δ = 0.1. These results highlight that the present deposition process leads to continuous and crack-free film of highly oxidized $Pr_4Ni_3O_{10+\delta}$ film.

4. Concluding Remarks

Polycrystalline $Pr_4Ni_3O_{10}$ coatings were obtained by combining RF magnetron co-sputtering with an appropriate annealing treatment under oxygen flux. The influence of the sputtering parameter on the composition is brought out. The stability of the $Pr_4Ni_3O_{10}$ crystal structure under oxygen was found to range between 1000°C and 1050°C. Above this temperature, $Pr_4Ni_3O_{10}$ phase turns into a Pr_2NiO_4 structure. $Pr_4Ni_3O_{10}$ crystallizes in orthorhombic structure with *Fmmm* space group. By combining working pressure and substrate temperature during the sputtering process we show that it is possible to monitor the microstructure of the sample leading to smooth and dense samples with controlled porosity and grain size. Electrical resistivity of ~$6.5.10^{-3}$ Ω.cm and the Seebeck coefficient of ~ – 23 μV.K^{-1} at 150°C highlight obtaining highly oxidized continuous coatings. These properties will be further investigated by the preparation and study of half solid oxide fuel synthetized with the sputtering process.

Acknowledgments

The authors thank Dr. Cécile Autret for help during X ray diffraction and Mr. Frédéric Dorvaux for help during sample deposition. The authors wish to thank Mrs. Christine Farmer for linguistic insight.

References

[1] P. Lacorre, J. B. Torrance, J. Pannetier, S. A. I. Nazzal, P. W. Wang, T. C. Huang, Synthesis, crystal structure, and properties of metallic $PrNiO_3$: Comparison with metallic $NdNiO_3$ and semiconducting $SmNiO_3$, J. Solid State Chem. 91 (1991) 225-237.
doi.org/10.1016/0022-4596(91)90077-U

[2] M. Zaghrioui, A. Bulou, P. Lacorre and P. Laffez, Electron diffraction and Raman scattering evidence of a symmetry breaking at the metal-insulator transition of $NdNiO_3$, Phys. Rev. B 64 (2001) 081102.
doi.org/10.1103/PhysRevB.64.081102

[3] A. Sediri, M. Zaghrioui, A. Barichard, C. Autret, B. Negulescu, L. Del Campo, P. Echegut , P. Laffez, Growth of polycrystalline $Pr_2NiO_{4+\delta}$ coating on alumina substrate by RF magnetron co-sputtering from composite targets, Thin Solid Films 600 (2016) 131–135.
doi.org/10.1016/j.tsf.2016.01.023

[4] A. Yamada, Y. Suzuki, K. Saka, M. Uehara, D. Mori, R. Kanno, T. Kiguchi, F. Mauvy, and J.-C. Grenier, Ruddlesden-Popper-Type Epitaxial Film as Oxygen Electrode for Solid-Oxide Fuel Cells, Adv. Mater. 20 (2008) 4124. doi.org/10.1002/adma.200801199

[5] C. Ferchaud, J-C Grenier, Y Zhang-Steenwinkel, M M.A van Tuel, F. P. F. van Berkel J.-M. Bassat, High performance praseodymium nickelate oxide cathode for low temperature solid oxide fuel cell, J. Power Sources 196 (2011) 1872-1879.
doi.org/10.1016/j.jpowsour.2010.09.036

[6] A. Jacobson, Materials for Solid Oxide Fuel Cells, Chem. Mat. 22 (2010) 660.
doi:10.1021/cm902640j

[7] Z. Zhang, M. Greenblatt, Synthesis, Structure, and Properties of $Ln_4Ni_3O_{10-\delta}$ (Ln = La, Pr, and Nd), J. Solid State Chem. 117 (1995), 236-246.
doi:10.1006/jssc.1995.1269

[8] J. Dailly, S. Fourcade, A. Largeteau, F. Mauvy, J.C. Grenier, M. Marrony, Perovskite and A_2MO_4-type oxides as new cathode materials for protonic solid oxide fuel cells, Electromchemica Acta 22 (2010) 5847–5853.
doi:10.1016/j.electacta.2010.05.034

[9] J. Fondard A. Billard G. Bertrand, P. Briois, $Ln_2NiO_{4+\delta}$ (Ln = La, Pr, Nd) coatings deposited by reactive magnetron sputtering as cathode material for intermediate temperature solid oxide fuel cell, Vacuum 152 (2018) 97-108.
doi.org/10.1016/j.vacuum.2018.03.013

[10] G. Amow, I.J. Davidson, S.J., A comparative study of the Ruddlesden-Popper series, $La_{n+1}Ni_nO_{3n+1}$ (n=1, 2 and 3), for solid-oxide fuel-cell cathode applications, Solid State Ionics 177 (2006) 1205–1210.
doi:10.1016/j.ssi.2006.05.005

[11] R. K. Sharma, M. Burriel, E. Djurado, $La_4Ni_3O_{10-\delta}$ as an efficient solid oxide fuel cell cathode: electrochemical properties versus microstructure, J. Mater. Chem. A 3 (2015) 23833–23843. doi:10.1039/c5ta07862h

[12] A.V. Kovalevsky, V.V. Kharton, A.A. Yaremchenko, Y.V. Pivak, E.N. Naumovich, J.R. Frade, Stability and oxygen transport properties of $Pr_2NiO_{4+\delta}$ ceramics, J. Amer. Ceram. Soc. 27 (2007) 4269-4272.
doi:10.1016/j.jeurceramsoc.2007.02.136

[13] V. Vibhu, J.-. Bassat, A. Flura, C. Nicollet, J.-C. Grenier and A. Rougier, Influence of La/Pr Ratio on the Ageing Properties of $La_{2-x}Pr_xNiO_{4+\delta}$ as Cathodes in IT-SOFCs, ECS Trans. 68, 2015, 825-835.
doi: 10.1149/06801.0825ecst

[14] V. Vibhu, A. Rougier, C. Nicollet, A. Flura, S. Fourcade, N. Penin, J-C. Grenier, J-M. Bassat, $Pr_4Ni_3O_{10+\delta}$: A new promising oxygen electrode material for solid oxide fuel cells, J. Power Sources 317 (2016) 184-193.
doi:10.1016/j.jpowsour.2016.03.012

[15] CELREF, LMGP-Suite Suite of Programs for the interpretation of X-ray Experiments, by Jean Laugier and Bernard Bochu, ENSP/Laboratoire des Matériaux et du Génie Physique, BP 46. 38042 Saint Martin d'Hères, France. http://www.inpg.fr/LMGP and http://www.ccp14.ac.uk/tutorial/lmgp/

[16] Ohring, Material Science of Thin Films, Academic press ISBN 0-12-52-4990-X.

[17] International Centre for Diffraction Data PDF card n°01-071-0341

[18] International Centre for Diffraction Data PDF card n°00-004-0835

[19] International Centre for Diffraction Data PDF card n°00-050-0468

[20] International Centre for Diffraction Data PDF card n°00-050-0243

[21] International Centre for Diffraction Data PDF card n°00-058-0850

[22] I. B. Sharma and D. Singh, Solid State Chemistry of Ruddlesden-Popper type complex Oxide, Bull. Mater. Sci. 21 (1998) 363.

[23] N.B. Pilling, R. E. Bedworth, "The Oxidation of Metals at High Temperatures". J. Inst. Met 29 (1923) 529-59

[24] J. A. Thornton, Influence of apparatus geometry and deposition conditions on the structure and topography of thick sputtered coatings, J. Vac. Sci. Technol. 11 (1974) 666.
doi:10.1116/1.1312732

[25] A. Boileau, F. Capon, P. Laffez, S. Barrat, J. L. Endrino, R. Escobar Galindo, D. Horwat, J. F. Pierson, Mechanisms of Oxidation of $NdNiO_{3-\delta}$ Thermochromic Thin Films Synthesized by a Two-Step Method in Soft Conditions, J. Phys. Chem. C 118 (2014) 5908-5917.
doi.org/10.1021/jp4111597

[26] J.-M. Bassat, C. Allançon, P. Odier, J.-P. Loup, M. Deus Carvalho, A. Watiaux, Electronic properties of $Pr_4Ni_3O_{10\pm\delta}$, Eur. J . Solid State Inorg. Chem. 35 (1998) 173.
doi.org/10.1016/S0992-4361(98)80195-1

Figure caption

Figure 1 X-ray diffraction versus temperature showing the crystallization of $Pr_4Ni_3O_{10}$ in the range 50°C-1200°C.

Figure 2 GI-XRD patterns of (a) bare YSZ substrate and (b-e) coatings deposited at room temperature and at (a-b) 1.5 Pa, (c) 0.5 Pa and (d) 5 Pa. Coatings (b) and (c-e) were annealed at 1000 °C/18 h and 1025 °C/18 h, respectively. $Pr_4Ni_3O_{10}$ peaks are indexed in the orthorhombic system. YSZ and sample holder, Pr_6O_{11}, NiO and an unknown phase are marked by ○, ◊, ▼ and ■ symbols, respectively.

Figure 3 a) and b) [010] and [101] Electron Diffraction patterns of $Pr_4Ni_3O_{10}$ crystal scratched from the thin film. The *Fmmm* space group conditions are confirmed and a *c* cell parameter close to 27.3Å can be measured, c) Typical size of the grains evidenced in the $Pr_4Ni_3O_{10}$ thin films, d) Lattice image showing the good crystallinity of the films and the stacking of the NiO layers. Here the light grey lines are representative of the NiO layers for $R_{n+1}Ni_nO_{3n+1}$ with n=3 (highlighted by 3 arrows).

Figure 4 (a-b) electron SEM micrographs of the $Pr_4Ni_3O_{10}$ coating deposited at room temperature and 1.5 Pa : (a) plan view Secondary Electron Image (SEI) and (b) Cross-section Backscattered Image. (c-d) plan views SEI-SEM micrographs of the $Pr_4Ni_3O_{10}$ coatings deposited at room temperature at 0.5 Pa and 5 Pa respectively. (e-f) plan views SEI-SEM micrographs of the $Pr_4Ni_3O_{10}$ coating deposited at 1.5 Pa at 400°C and 600°C, respectively. All samples were annealed at 1025°C/18 h in O_2 flow. Inset in figure 4a shows plane view SEI-SEM of YSZ bare substrate.

Figure 5 Evolution of the electrical conductivity and Seebeck coefficient as a function of temperature for a $Pr_4Ni_3O_{10}$ film deposited at 1.5 Pa and room temperature followed by annealing at 1025°C/18 h in O_2 flow.

Figure 1 Laffez et al

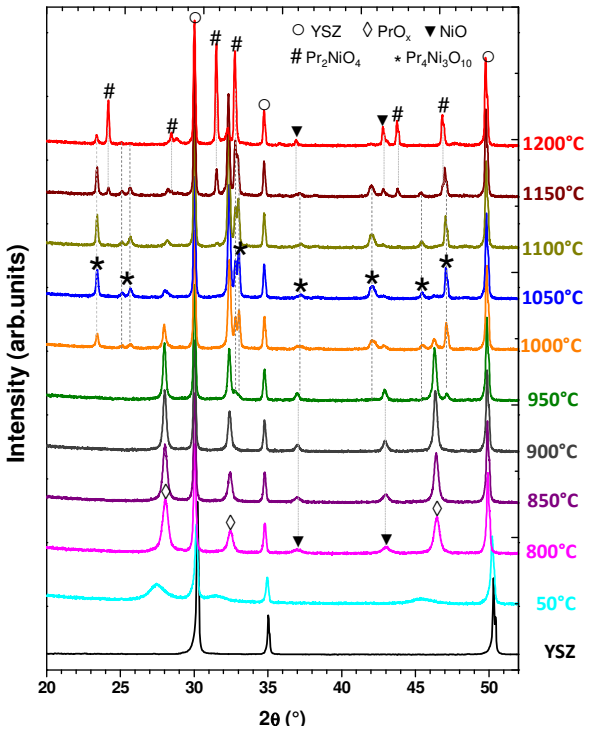

Figure 1 X ray diffraction versus temperature showing the crystallization of $Pr_4Ni_3O_{10}$ in the range 50°C-1200°C.

Figure 2 Laffez et al

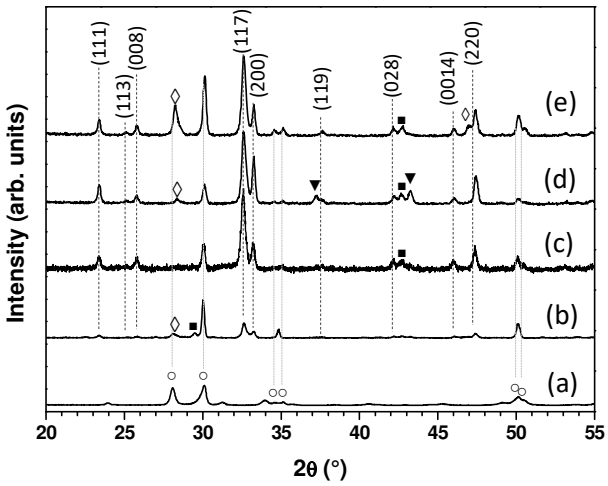

Figure 2 GI-XRD patterns of (a) bare YSZ substrate and (b-e) coatings deposited at room temperature and at (a-b) 1.5 Pa, (c) 0.5 Pa and (d) 5 Pa. Coatings (b) and (c-e) were annealed at 1000 °C/18 h and 1025 °C/18 h, respectively. $Pr_4Ni_3O_{10}$ peaks are indexed in the orthorhombic system. YSZ and sample holder, Pr_6O_{11}, NiO and an unknown phase are marked by ○, ◊, ▼ and ■ symbols, respectively.

Figure 3 Laffez et al

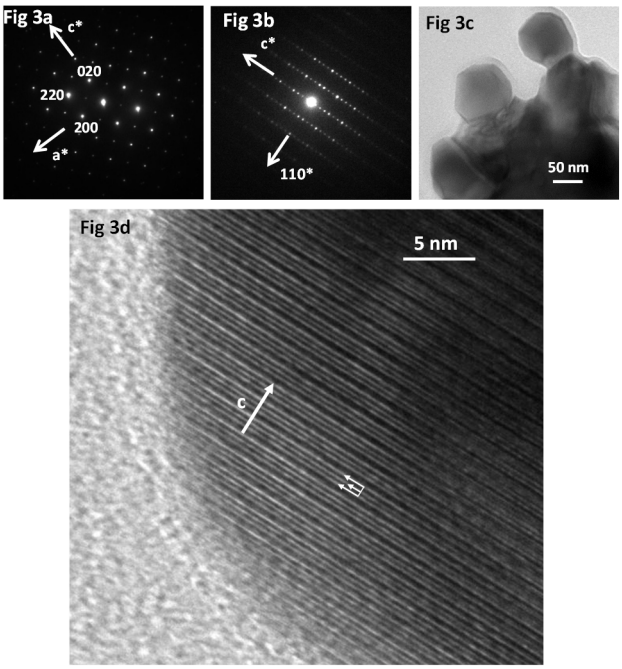

Figure 3 a) and b) [010] and [101] Electron Diffraction patterns of $Pr_4Ni_3O_{10}$ crystal scratched from the thin film. The *Fmmm* space group conditions are confirmed and a *c* cell parameter close to 27.3Å can be measured, c) Typical size of the grains evidenced in the $Pr_4Ni_3O_{10}$ thin films, d) Lattice image showing the good crystallinity of the films and the stacking of the NiO layers. Here the light grey lines are representative of the NiO layers for $R_{n+1}Ni_nO_{3n+1}$ with n=3 (highlighted by 3 arrows).

Figure 4 Laffez et al

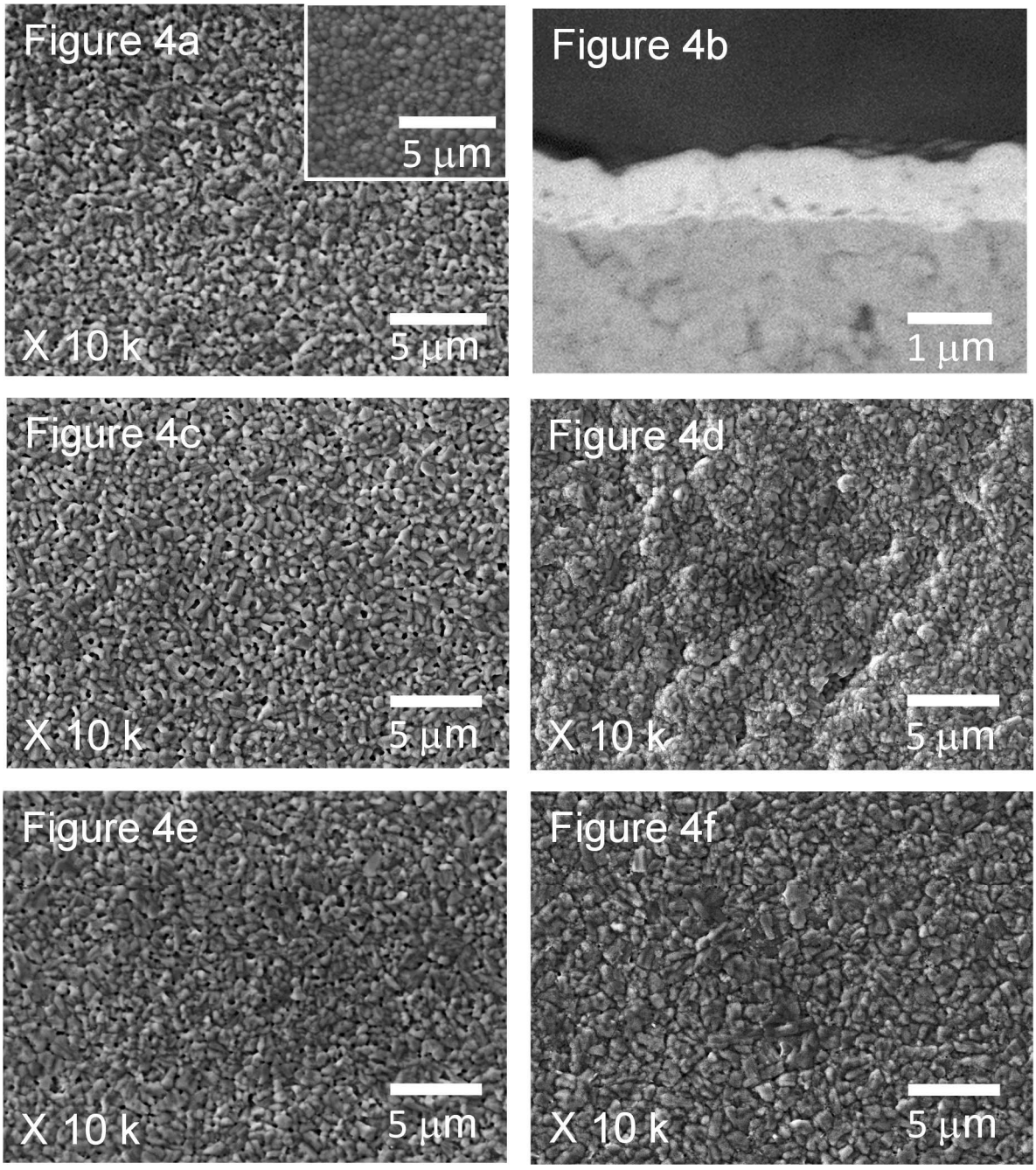

Figure 4 (a-b) electron SEM micrographs of the $Pr_4Ni_3O_{10}$ coating deposited at room temperature and 1.5 Pa : (a) plan view Secondary Electron Image (SEI) and (b) Cross-section Backscattered Image. (c-d) plan views SEI-SEM micrographs of the $Pr_4Ni_3O_{10}$ coatings deposited at room temperature at 0.5 Pa and 5 Pa respectively. (e-f) plan views SEI-SEM micrographs of the $Pr_4Ni_3O_{10}$ coating deposited at 1.5 Pa at 400°C and 600°C, respectively. All samples were annealed at 1025°C/18 h in O_2 flow. Inset in figure 4a shows plane view SEI-SEM of YSZ bare substrate.

Figure 5 Laffez et al

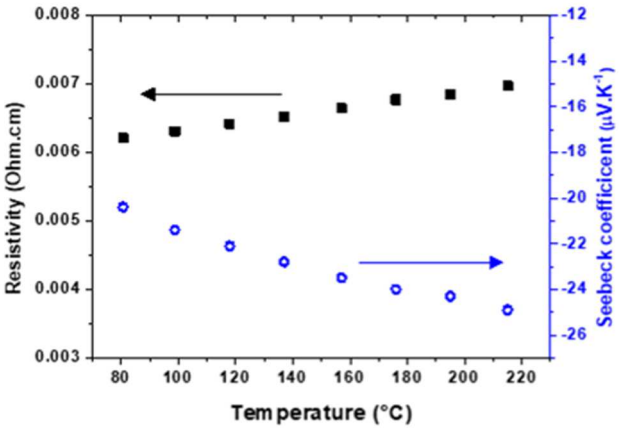

Figure 5 Evolution of the electrical conductivity and Seebeck coefficient as a function of temperature for a $Pr_4Ni_3O_{10}$ film deposited at 1.5 Pa and room temperature followed by annealing at 1025°C/18 h in O_2 flow.

Table 1 Laffez et al

Substrate	Pr Power	Pr Voltage	Ni Power	Ni Voltage	% Pr	%Ni
Al_2O_3	100	267	80	147	55	45
Al_2O_3	40	108	20	250	55	45
YSZ	40	110	28	283	53	47

Table 1 : Typical sputtering parameters leading to the stoichiometric composition of $Pr_4Ni_3O_{10}$

Table 2 Laffez et al

Annealing temperature	a (Å)	b (Å)	c (Å)
1000 °C	5.372(6)	5.478(12)	27.50(4)
1025 °C	5.3723(18)	5.4616(19)	27.525(10)

Table 2 : Refined cell parameters of the annealed $Pr_4N_3O_{10}$ coating using *Fmmm* space group (in parenthesis is the standard deviation).